ACS APPLIED MATERIALS & INTERFACES

Research Article

www.acsami.org

Enzyme Catalytic Efficiency: A Function of Bio−Nano Interface Reactions

Alan S. Campbell,[†] Chenbo Dong,[†] Fanke Meng,[‡] Jeremy Hardinger,[†] Gabriela Perhinschi,[†] Nianqiang Wu,[‡] and Cerasela Zoica Dinu*,[†]

[†]Department of Chemical Engineering and [‡]Department of Mechanical and Aerospace Engineering, West Virginia University, Morgantown, West Virginia 26506, United States

Supporting Information

ABSTRACT: Biocatalyst immobilization onto carbon-based nanosupports has been implemented in a variety of applications ranging from biosensing to biotransformation and from decontamination to energy storage. However, retaining enzyme functionality at carbon-based nanosupports was challenged by the non-specific attachment of the enzyme as well as by the enzyme−enzyme interactions at this interface shown to lead to loss of enzyme activity. Herein, we present a systematic study of the interplay reactions that take place upon immobilization of three pure enzymes namely soybean peroxidase, chloroperoxidase, and glucose oxidase at carbon-based nanosupport interfaces. The immobilization conditions involved both single and multipoint single-type enzyme attachment onto single and multi-walled carbon nanotubes and graphene oxide nanomaterials with properties determined by Fourier transform infrared spectroscopy (FTIR), energy dispersive X-ray analysis (EDX), scanning electron microscopy (SEM), and atomic force microscopy (AFM). Our analysis showed that the different surface properties of the enzymes as determined by their molecular mapping and size work synergistically with the carbon-based nanosupports physico-chemical properties (i.e., surface chemistry, charge and aspect ratios) to influence enzyme catalytic behavior and activity at nanointerfaces. Knowledge gained from these studies can be used to optimize enzyme−nanosupport symbiotic reactions to provide robust enzyme-based systems with optimum functionality to be used for fermentation, biosensors, or biofuel applications.

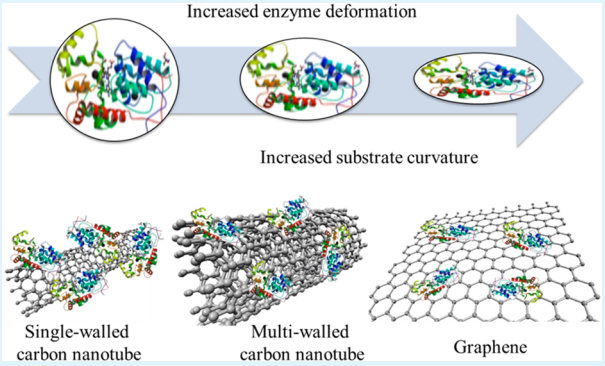

KEYWORDS: *enzyme immobilization, bio−nano interface, symbiotic behavior, catalytic tuning*

INTRODUCTION

Enzymes are a naturally occurring class of proteins that possess unique properties including high catalytic activity, selectivity, and specificity. Enzymes are environmentally friendly and produce fewer harsh byproducts than their chemical counterparts.[1,2] Because of such properties, enzymes are now key players in various industrial processes from waste treatment[3,4] to food processing[5] and from biodiesel production[6] to the petroleum refining industry.[7] More recently, enzyme-based conjugates obtained by immobilization of enzymes onto nanoscale solid supports have shown applicability in biosensing,[8,9] drug delivery,[10] and decontamination.[11,12] In particular, Besteman et al. reported on the use of single-walled carbon nanotubes as supports for immobilization of glucose oxidase for biosensing applications,[13] Luckarift et al. examined the use of biomimetic silica supports for butyrylcholinesteras immobilization for flow through reactors,[14] and Fernandez-Lafuente et al. showed that coupling immobilization and site-directed mutagenesis can improve biocatalyst or biosensor performance,[15] while Dinu et al. reported on immobilization of enzyme perhydrolase S54 V onto carbon nanotubes to be used for generating decontamination platforms.[11]

In a favorable nanoenvironment, enzyme immobilization was shown to lead to increased enzyme stability and improved specificity[1,2,16] and allowed for prolonged enzyme functionality through chemical (e.g., cross-linking)[17] and physical treatment (e.g., pH enhancement or lyophilization).[18] For instance, immobilization onto carbon-based nanosupports was shown to increase enzyme turnover and to allow for prolonged enzyme-based conjugate usage.[11,17,19] Nanosupport immobilization studies have also proved that, while the high aspect ratio of the nanosupports allows enzyme-based conjugate retention in solution, multiple usages and ease of conjugate recovery via filtration, the nonspecific binding of the enzyme at the nanointerface can result in enzyme active site deformation (i.e., change in the active site conformation)[19] and thus increased enzyme−nanosupport interactions with subsequent reduced enzyme activity.[16,19−22] Future developments in enzyme-based applications of enzyme-based-nano conjugates need to account for increased enzyme functionality, high operational stability,

Received: June 28, 2013
Accepted: March 25, 2014
Published: March 25, 2014

   dx.doi.org/10.1021/am500773g | ACS Appl. Mater. Interfaces 2014, 6, 5393−5403

efficiency, yield of recovery and conversion, and reduced enzyme inhibition. However, while previous examples show that a significant amount of research has been directed towards understanding the interactions of known enzymes with nanosupports, the molecular mechanisms and synergistic reactions that take place at the nanosupport interface upon enzyme immobilization have yet to be fully understood.

We hypothesized that fine control of the enzyme−nanosupport interface through the control of the enzyme immobilization process as well as nanosupport characteristics can lead to enhanced enzyme catalytic efficiency. To test our hypothesis, we used pure glycosylated enzymes with different properties (e.g., surface chemistry, molecular weight, isoelectric point, etc.), nanosupports with different characteristics (both physical and chemical), and different immobilization techniques (i.e., physical or chemical). Specifically, soybean peroxidase (SBP), an anionic monomeric glycoprotein (pI 3.9)[23] with a molecular weight of ∼40 kDa[24] known for its unusual thermostability and a high oxidation potential, chloroperoxidase (CPO), a monomeric enzyme with a molecular weight of ∼42 kDa,[25] and glucose oxidase (GOx), a homodimer flavoenzyme oxidoreductase with a molecular weight of ∼180 kDa,[26] were used as models. The choice in enzymes was based on their extended applications with SBP being used for diagnostics[27−29] and waste-water treatment industrial implementation;[30−32] CPO for chiral organic synthesis,[33−35] decontamination,[36] and the petroleum industry,[37,38] and GO_X for biosensing,[39,40] biofuel cell formation,[41] and food processing applications.[42] The selected carbon-based nanosupports encompassed single-walled carbon nanotubes (SWCNTs), multi-walled carbon nanotubes (MWCNTs), and graphene sheets (GON) with different physical and chemical properties as demonstrated by Fourier transform infrared spectroscopy (FTIR), energy dispersive X-ray analysis (EDX), scanning electron microscopy (SEM), and atomic force microscopy (AFM). The choice of the nanosupports was based on their extended implementation in a wide variety of applications from biosensing[40,43] to large-scale industrial processing and waste remediation.[44−46] Lastly, the chosen immobilization techniques were aimed to offer different enzyme attachment mechanisms at nanointerfaces, namely single or multipoint attachment.[47−49]

Our systematic studies on the underlying mechanisms that control enzyme activity and catalytic behavior at nanointerfaces seek to reveal whether there is an optimum support to be used for a specific enzyme immobilization in order to lead to maximum catalytic efficiency of that enzyme. Discovering an optimum strategy that could be used in the future when the formation of bio−nano conjugate systems with increased enzyme functionality is considered can fill the gap in developing robust enzyme-based systems with applications in fermentation, biosensoring, or biofuel production.

MATERIALS AND METHODS

Graphene Oxide Nanosheet Synthesis. Graphene oxide nanosheets (GON) were produced from graphite powder (Alfa Aesar, 99.8% purity). First, 10 g of the graphite powder and 5 g of sodium nitrate ($NaNO_3$, Sigma Aldrich, 99.0%) were added to 230 mL of concentrated sulfuric acid (H_2SO_4, Fisher Scientific, 96.4%) in a 2000 mL flask; the flask was subsequently placed in an ice bath and the mixture was stirred slowly. A 30 mg portion of potassium permanganate ($KMnO_4$, Sigma Aldrich, 99.0%) was added slowly to the flask to ensure that the temperature of the mixture remained below 20 °C. Next, the solution was heated to 35 °C for 30 min, diluted in 460 mL of deionized (DI) water, and again quickly heated to 98 °C for 15 min. The mixture was subsequently rediluted in 710 mL of DI water, preheated to 35 °C, and incubated with 30 mL of 30% hydrogen peroxide (H_2O_2, Sigma Aldrich). Finally, the solution was filtered and washed using DI water at 35 °C until the effluent was clear and the pH was kept constant at 6. The resulting product was dried in a vacuum oven; the obtained brown powder was stored at room temperature for future use.

Carbon-Based Material Acids Treatment. Functionalized carbon-based materials (CMATs; SWCNTs, 85% purity, Unidym Inc.; MWCNTs, 95% purity, NanoLab Inc.; or GON) were prepared via acids treatment as previously described.[50] Briefly, 100 mg of pristine CMATs were added to a 60 mL mixture of 3:1 (V:V) H_2SO_4 and nitric acid (HNO_3, Fisher Scientific, 69.6%). The mixture was ultrasonicated for 6 h (Branson 2510, Fisher Scientific) at a constant temperature of approximately 23 °C. Next, the solution was diluted in DI water and filtered through a GTTP 0.2 μm polycarbonate membrane (Fisher Scientific). Several cycles of redispersion and filtration in DI water were performed to remove acidic residues or catalysts and impurities. The CMATs isolated on the filter membrane were dried in a vacuum desiccator and stored at room temperature until use.

CMATs Characterization. Chemical structure, morphology, and elemental composition of CMATs were investigated using Fourier transform infrared spectroscopy (FTIR), scanning electron microscopy (SEM), and energy-dispersive x-ray spectroscopy (EDX), respectively. For FTIR, 2 mg pellets of samples were collected and analyzed under the transmission mode by using KBr pellet on a Thermo Nicolet Instrument. For SEM and EDX characterizations, samples (1 mg/mL in DI water) were deposited on silica wafers and dried under vacuum. Experiments were performed on a Hitachi S-4700 field emission scanning electron microscope with a S-4700 detector combining secondary (SE) and backscattered (BSE) electron detection (in a single unit).

The length of pristine and acids treated SWCNTs and MWCNTs were quantified using atomic force microscopy (AFM) and a silicon tip (Asylum Research, 50-90 kHz AC240TS) operating in air tapping mode. Briefly, nanotube samples in DI water (0.1 mg/mL) were deposited onto mica surfaces (9.5 mm diameter, 0.15−0.21 mm thickness, Electron Microscopy Sciences) and dried overnight under vacuum. Scans of 10 μm × 10 μm and 1 μm × 1 μm areas were acquired.

To evaluate the CMATs' degree of hydrophilicity/hydrophobicity, dispersity tests were performed in DI water (pH 6.25), phosphate buffered saline (PBS, 100 mM, pH 7, Sigma Aldrich), and citric acid buffer (CAB 50 mM, pH 4.8, Sigma Aldrich). Briefly, CMATs were first dispersed in each of the different solvents at a concentration of 3 mg/mL. The suspension was subsequently centrifuged at 3000 rpm for 5 min and 0.8 mL of the generated supernatant was removed and filtered through the GTTP 0.2 μm polycarbonate filter membrane. The filter was subsequently dried under vacuum, and the amount of CMATs on the filter was weighed. Dispersity was calculated based on the volume suspended, the initial amount used in the dispersion test, and the final amount isolated on the filter paper.

Enzyme Immobilization. Soybean peroxidase (pure SBP, Bioresearch, $R_z = 2$), glucose oxidase (pure GO_X, Type VII, Sigma, $R_z = 1.3$), and chloroperoxidase (pure CPO, Bioresearch, $R_z = 1.3$) were immobilized onto CMATs using either physical or covalent binding.

For physical binding 2 mg of CMATs were first dispersed in 2 mL of enzyme solution (1 mg/mL in PBS for SBP, 0.5 mg/mL in PBS for GO_X, or 0.5 mg/mL in CAB for CPO) via brief sonication. The solution was then incubated at room temperature for 2 h with shaking at 200 rpm. Next, the enzyme−CMAT conjugates were recovered by filtration through the GTTP 0.2 μm polycarbonate filter membrane. The supernatant was isolated and its volume recorded. The conjugates isolated on the filter were washed at least 6 times using the corresponding buffer (2 mL for each wash) to remove loosely bound enzyme, with the first two washes being isolated and their volumes recorded. Finally, the conjugates were redispersed in 2 mL of their corresponding buffer and stored at 4 °C.

For covalent binding, 2 mg of CMATs were first activated using 1-ethyl-3-[3-dimethylaminopropyl] carbodiimide (EDC, Acros Organics) and *N*-hydroxysuccinimide (NHS, Pierce) chemistry. Specifically, CMATs were dispersed via sonication in 160 mM EDC and 80 mM

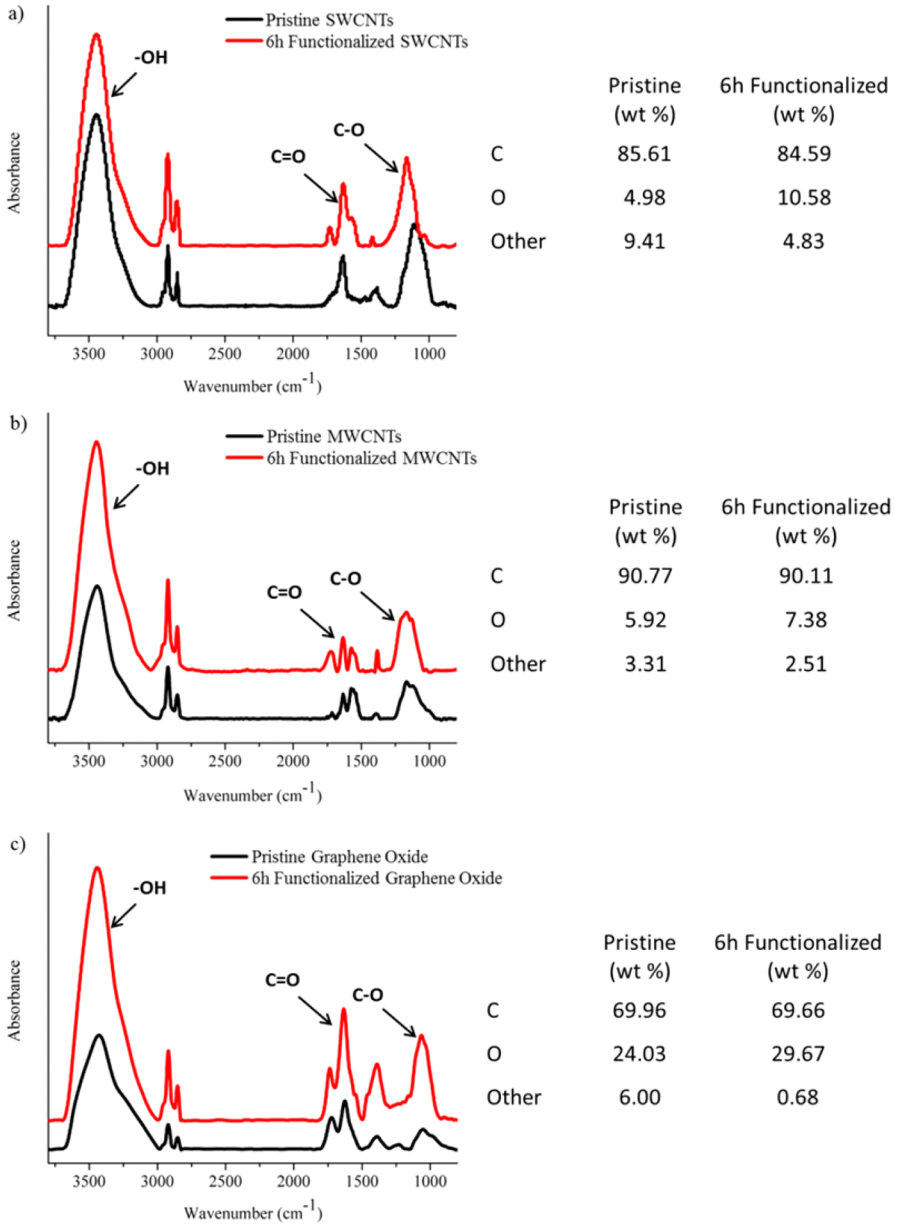

Figure 1. Characterization of carbon-based materials (CMATs). FTIR and EDX spectra analysis of (a) pristine and acid-functionalized SWCNTs, (b) pristine and acid-functionalized MWCNTs, and (c) pristine and acid-functionalized graphene oxide nanosheets (GON). FTIR and EDX spectra confirmed the presence of carboxyl (COOH) functionalizations upon acid mixture incubation of CMATs.

NHS in 2-(*N*-morpholino)ethanesulfonic acid sodium salt buffer (MES, 50 mM, pH 4.7) with a final volume of 2 mL and incubated at room temperature for 15 min with shaking at 200 rpm. Subsequently, the mixture was filtered through a GTTP 0.2 μm polycarbonate filter membrane and washed thoroughly with MES buffer to remove any ester residues. Next, the activated CMATs were immediately dispersed in 2 mL of the selected enzyme solution (consistent with physical binding) and incubated at room temperature for 3 h with shaking at 200 rpm. Enzyme−CMAT conjugates were then recovered and washed, with the supernatant, and the two washes were recovered (consistent with physical binding). Finally, the conjugates were redispersed in 2 mL of the corresponding buffer and stored at 4 °C.

For covalent binding through a spacer, 2 mg of the selected CMATs were first activated using EDC/NHS chemistry as previously described (see covalent binding), subsequently dispersed in 5 mL of 1 mg/mL Amino-dPEG$_8$-COOH (PEG, 32.2 Å, Quanta Biodesign) in the designated buffer, and incubated at room temperature for 3 h with shaking at 200 rpm. The resulting conjugates were then filtered and washed with their corresponding buffer. Finally, the selected enzyme was attached to the PEG linker as previously described. After the time elapsed, enzyme−PEG−CMAT conjugates were recovered and washed, and the supernatant and the two washes were recovered to quantify the enzyme loading (consistent with physical and covalent binding). Conjugates were redispersed in 2 mL of their corresponding buffer and stored at 4 °C.

Covalent binding was confirmed by incubating the enzyme-carbon-based conjugates in 1 M NaCl solution for 10 min at 200 rpm; upon incubation, the conjugates were filtered using the GTTP 0.2 μm polycarbonate filter membrane and washing thoroughly with their corresponding buffers. The resulting supernatant and washes were recovered to evaluate any enzyme removal.

Enzyme Loading onto CMATs. The amount of the immobilized enzyme relative to the amount of CMATs being used (i.e., the enzyme loading) was estimated using standard BCA Assay (Pierce) and subtracting the amount of enzyme washed out in the supernatant and the first two washes (see above) from the initial amount of enzyme

dx.doi.org/10.1021/am500773g | *ACS Appl. Mater. Interfaces* 2014, 6, 5393−5403

added during the immobilization process. Briefly, 1 mL of working reagent containing 50 parts reagent A with 1 part reagent B (reagents were provided stock with the BCA Assay kit) was mixed with 50 μL of enzyme solution (either from the supernatant or the washes) and incubated at 37 °C for 30 min. Absorbance at 562 nm was recorded for each sample using a UV−vis spectrophotometer (Thermo Scientific EVO300) and compared to a calibration curve of known concentrations of the respective enzyme (free in solution) in the working reagent. Loadings were estimated as the difference between the amount of enzyme washed out from the initial amount of enzyme added during the incubation relative to the amount of CMATs being used.

Determine the Specific Retained Activity of the Enzyme Immobilized Onto CMATs. Immobilized enzyme retained specific activity was determined using colorimetric reactions monitored on a UV−vis spectrophotometer (Thermo Scientific EVO300). The specific activity was calculated by comparing the activity of immobilized enzyme to the activity of free enzyme in solution at the same amount. Specifically, the specific activity of SBP was determined by monitoring the oxidation of 2,2′-azinobis[3-ethylbenzothiazoline-6-sulfonic acid] (ABTS, Sigma Aldrich) by SBP in the presence of H_2O_2 (Sigma Aldrich) at 412 nm. Briefly, 20 μL of the SBP solution to be tested (free or immobilized) was added to 650 μL of 0.25 mg/mL ABTS and mixed in a plastic cuvette. Next, 20 μL of 6.5 mM H_2O_2 was added to the mixture to initiate the reaction, and the cuvette was immediately placed on the spectrophotometer; the rate of absorbance change was monitored for 2 min. The initial reaction rate was calculated from the time-course slope and reported in micromolar per microgram second.

For the specific activity of GO_X, 400 μL of PBS, 250 μL of 0.25 mM glucose (Across), 250 μL of 0.25 mg/mL ABTS, and 50 μL of 0.5 mg/mL SBP were first mixed in a plastic cuvette. Then, 50 μL of the GO_X solution to be tested was added to initiate the reaction and the cuvette was immediately placed in the spectrophotometer; the rate of absorbance change was monitored for 2 min. The initial reaction rate was calculated from the time-course slope and reported in micromolar per microgram second.

The specific activity of CPO was determined by monitoring the conversion of 2-chloro-5,5-dimethyl-1,3-cyclohexanedione (monochlorodimedon, Alfa Aesar) to dichlorodimedon by CPO in the presence of Cl^- and H_2O_2 at 278 nm. Briefly, 500 μL of CAB, 440 μL of 227.27 mM NaCl (ACROS), 20 μL of 5 mM monochlorodimedon, and 20 μL of the CPO sample to be tested were first mixed in a quartz cuvette. Then, 20 μL of 50 mM H_2O_2 was added to initiate the reaction and the cuvette was immediately placed in the spectrophotometer; the rate of absorbance change was monitored for 2 min. The initial reaction rate was calculated from the time-course slope and reported in micromolar per microgram second.

Enzyme Kinetic Parameters Determination. The kinetic parameter, K_m (where K_m is the Michaelis−Menten constant in micromolar), V_{max} (where V_{max} represents the maximum rate of reaction in micromolar per microgram second), and k_{cat} (enzyme turnover, 1/s), values of the free and immobilized enzyme were determined by measuring the initial rates of reaction in the respective activity assays (as described above), with varying substrate concentrations and using nonlinear regression. Specifically, for SBP the concentration of H_2O_2 was varied from 0 to 0.04 mM, for GO_X the concentration of glucose was varied from 0 to 100 mM, and for CPO the concentration of H_2O_2 was varied from 0 to 4 mM.

Statistical Analysis. All results are presented as mean ± standard deviation with at least six trials for each conjugate.

RESULTS AND DISCUSSION

Morphology and Structure Characterization of Carbon-Based Materials (CMATs). Pristine SWCNTS (diameter = 0.8−1.2 nm, length = 760 ± 276 nm), pristine MWCNTs (diameter = 10−20 nm, length = 6049 ± 2954 nm), and pristine GON (sheets of 500−5000 nm) were acids treated by incubation in a nitric and sulfuric acids mixture for 6 h[50] to generate nanosupports with different characteristics. To investigate whether acids treatment changed the physical and chemical properties of the pristine carbon-based materials (CMATs), we used Fourier transform infrared spectroscopy (FTIR), energy dispersive X-ray analysis (EDX), scanning electron microscopy (SEM), and atomic force microscopy (AFM).

Our FTIR analysis showed that acids treatment led to grafting of carboxyl (COOH) functionalities onto all the CMATs being tested. Specifically, the analysis of the chemical structure of both SWCNTs and MWCNTs (Figure 1a and b, respectively) showed a peak at 3450 cm^{-1} corresponding to the hydroxyl moiety and a ∼2900 cm^{-1} peak corresponding to the stretching mode of C—H groups. The 1750 cm^{-1} band corresponded to the C═O bond in the carbonyl and carboxylic moiety while the bands at 1550−1660 cm^{-1} were associated with the C—C bonds formation.[51] The bands in the 1300−950 cm^{-1} range were characteristic of C—O bond formation and, thus, confirmed the presence of large amounts of hydrated surface oxides and CMATs-COOH functionalization. The FTIR spectrum of the GON is shown in Figure 1c. The large peak in the 3400−3200 cm^{-1} range is indicative of formation of hydroxyl groups at the surface of the GON.[52] The peak at ∼1740 cm^{-1} is a result of the C═O bonds in the COOH groups as well as in carbonyl moieties, while the ∼1620 cm^{-1} peak confirmed the presence of C═C bonds resulted from unoxidized regions of the graphene. Finally, the large band at 1400−1060 cm^{-1} confirmed the presence of COOH groups in epoxy or alkoxy groups formed at the surface of the CMATs.[52]

EDX analysis (Figure 1, table format) further confirmed COOH functionalization of CMATs; specifically, the O content increased in the acids-treated CMATs while the C and other elements content decreased.[53] The decrease in other elements was a result of metal catalyst residues and other impurities being removed upon acid treatment as well as nanosupports being shortened thus leading to the formation of amorphous carbon.[50]

To confirm the shortening of the nanotubes we compared COOH-functionalized SWCNTs and MWCNTs with their pristine counterparts using tapping mode AFM. Our analysis showed that acid treatment reduced the length of SWCNTs from 760 ± 276 to 516 ± 277 nm and the length of MWCNTs from 6049 ± 2954 to 452 ± 213 nm. The diameters of the nanotubes were however unaffected by the treatment; similarly, the dimensions of the GON were maintained constant. Further, SEM showed no significant morphological changes for the acid-treated samples when compared to their pristine counterparts (Supporting Information Figure S1). Our results are in agreement with previous studies, which showed that liquid phase oxidation with a strong acid mixture introduces structural changes and adds free COOH groups to nanomaterials.[50,51,53]

Carboxyl functionalization upon acids treatment improved CMAT dispersity in several solvents (Supporting Information Table S1). Specifically, in DI water (pH 6.25), the dispersity of SWCNTs, MWCNTs, and GON improved by 9.3-, 6.8-, and 6.5-fold, respectively. Similarly, in PBS (pH 7) the dispersity of SWCNTs, MWCNTs, and GON improved by 4.8-, 3.8-, and 1.4-fold. Further, in CAB (pH 4.8) the dispersity of SWCNTs, MWCNTs, and GON improved by 8.3-, 9.3-, and 13.5-fold relative to their pristine counterparts. The increase in dispersity upon acids treatment is attributed to the increase in the number of COOH groups and thus increased carboxylate anion formation through deprotonation of these groups in water-based environments.[54] The poor dispersion observed at lower pH values (i.e., in CAB) can be attributed to the aggregation of CMATs through H bonding in these conditions.[55] The acids-treated MWCNTs and GON had the lowest dispersity in PBS

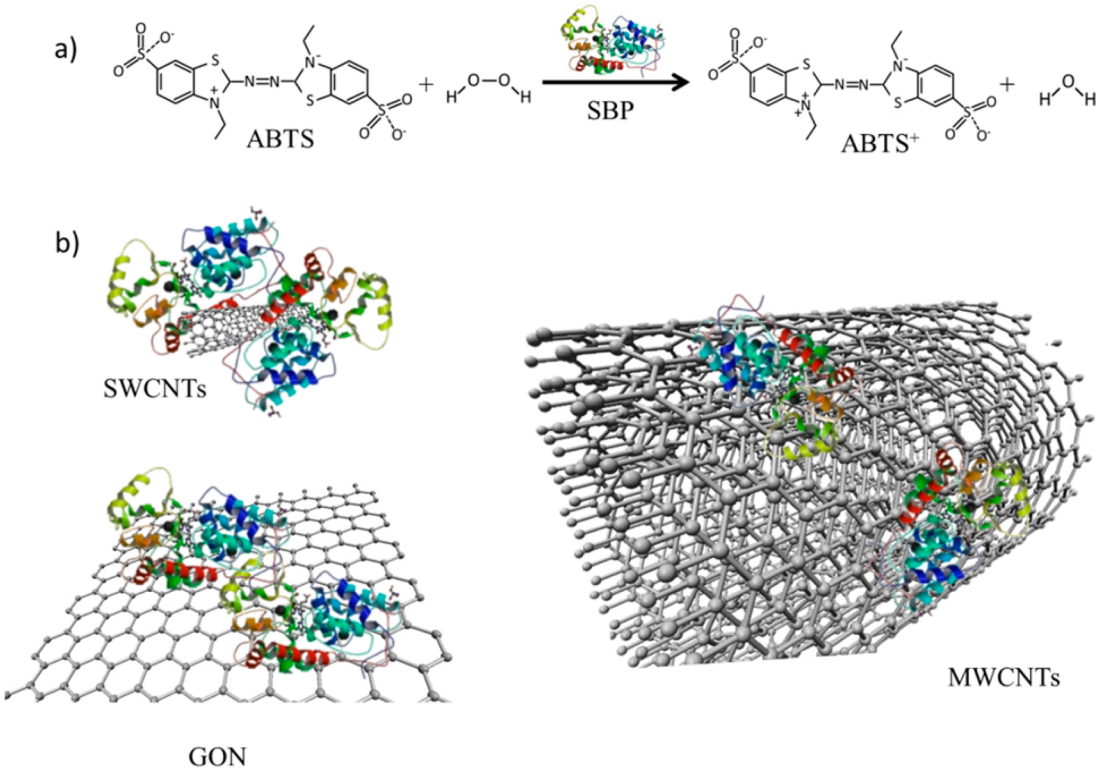

Figure 2. Concept schematic of soybean peroxidase (SPB) immobilization onto CMATs. (a) SBP catalyzes the oxidation of ABTS to ABTS$^+$. (b) SPB immobilization onto CMATs with different surface curvatures and aspect ratios led to enzyme-based conjugates.

presumably due to the higher ionic strength of this buffer that could have induced aggregation of their carboxylated anions.[55] This effect was not observed for SWCNTs since these nanotubes have a reduced number of defects and thus a lower rate of COOH functionalization relative to both MWCNTs and GON.

Influence of the Bio−Nano Interface on Enzyme Catalytic Behavior. Previously characterized CMATs were used as nanosupports for model enzyme soybean peroxidase (SBP) immobilization (SBP, Figure 2a); the high dispersity of the CMATs was required to ensure uniform loading of the nanosupports. The different radii of curvature of the CMATs were required to determine the geometrical congruence and thus the degree of enzyme−nanosupport interactions.[11,19,48]

Three independent immobilization techniques, i.e., physical adsorption, covalent binding, and covalent binding through a PEG linker, were used. The different immobilization techniques aimed to provide a variety of enzyme−nanosupport interactions. In particular, physical binding provides a multipoint attachment;[48,56] however, such a process was previously shown to lead to deformation of the enzyme (e.g., change in active's site conformation or change in the enzyme's footprint) at the nanointerface.[11] Covalent binding might reduce such deformation while theoretically serving as a zero-length single point attachment technique.[19,47,49,57] Lastly, covalent binding through an arm spacer could serve as a single-point immobilization method that brings the enzyme away from the nanosupport while increasing its substrate binding capability.[11,12] Figure 2b shows the concept of SBP immobilization onto the COOH-functionalized CMATs.

The amounts of SBP attached to the different CMATs relative to the amount of CMATs being used (i.e., the enzyme loadings) are shown in Supporting Information Table S2, while the specific retained activities of the enzyme-based conjugates relative to the enzyme loading is given in Figure 3a. Our data showed that the specific retained activity of the immobilized SBP varied significantly with the nanosupport being tested. In particular, SBP retained the highest specific activity when immobilized onto MWCNTs using covalent binding (about 28% retained specific activity relative to the free enzyme) while the lowest specific activity was displayed by the enzyme immobilized onto GON using covalent binding with PEG linker (about 1.6 % of the specific activity of the free enzyme). The highest specific activity for the physically bound SBP was observed for the enzyme immobilized onto MWCNTs (about 25 % of the specific activity of the free enzyme); however, the same immobilization method allowed retention of only about 15% and 1.7% specific activity onto SWCNTs and GON, respectively. Covalent immobilization also yielded to only about 4% of the specific activity of the free enzyme activity both onto SWCNTs and GON nanosupports, while covalent binding through the PEG linker led to the highest specific retained activity for the enzyme immobilized onto MWCNTs (about 20% of the specific activity of the free enzyme) and only about 8% and 1.6% onto SWCNTs and GON, respectively. Control experiments have been also performed to validate the feasibility of the covalent binding. Specifically, the enzyme-carbon-based nanosupports have been incubated in high salt concentrations known to remove the enzymes bound through nonspecific electrostatic interactions; subsequent evaluation of the enzyme loading showed that such high salt incubation removed <3% of the immobilized enzyme. However, upon such incubation, the remaining immobilized enzyme lost about 70% of its initial activity possibly due to the accelerated covalent multipoint attachment.[58]

Enzyme catalytic behavior at the different CMAT nanointerfaces was assessed under varying concentrations of hydrogen peroxide (Figure 3b−d); the kinetic parameters V_{max} (i.e., the

dx.doi.org/10.1021/am500773g | ACS Appl. Mater. Interfaces 2014, 6, 5393−5403

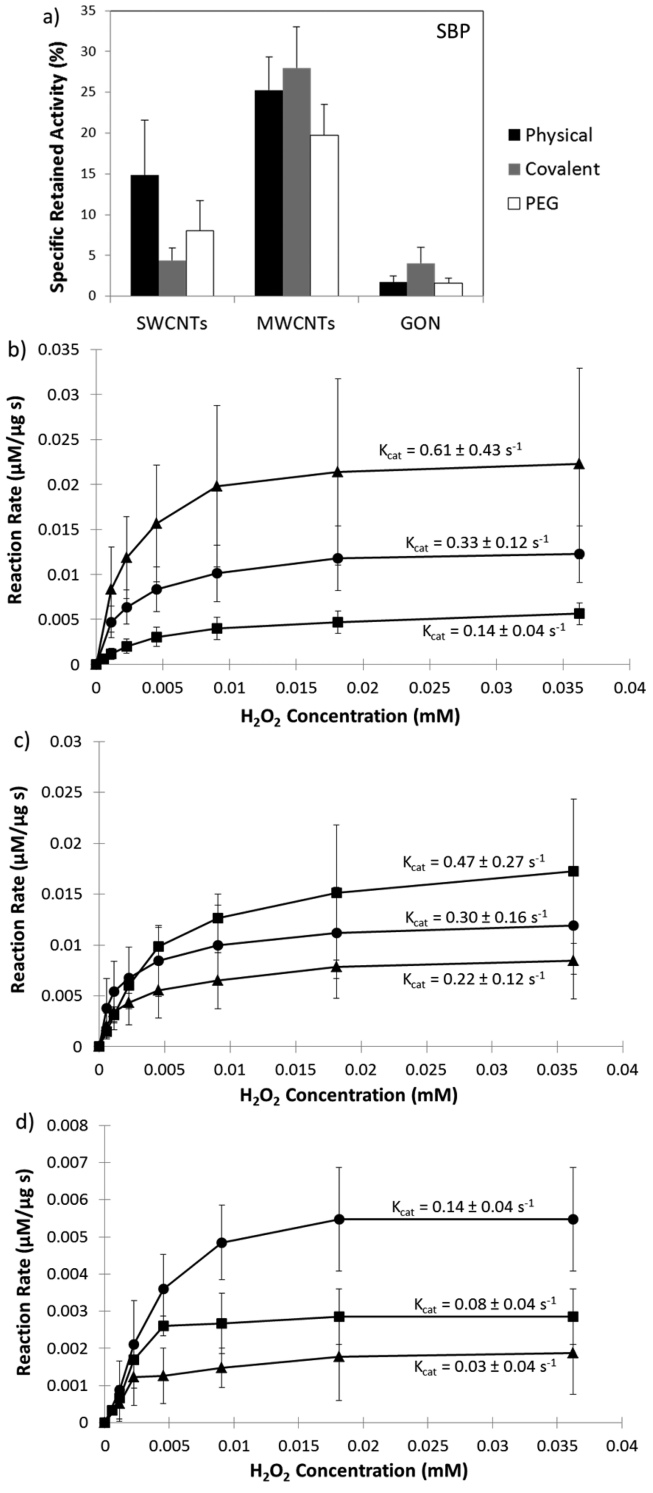

Figure 3. Catalytic behavior of model enzyme SBP immobilized onto different CMATs. (a) Comparison of the specific retained activity of SBP upon immobilization onto SWCNTs, MWCNTs, and GON. Physical adsorption, covalent binding, and covalent binding with a PEG linker were used. The nanosupport diameter increases from left to right. Michaelis–Menten kinetics data of SBP immobilized using physical adsorption (filled square), covalent binding (filled circle), and covalent binding via PEG linker (filled triangle) onto (b) SWCNTs, (c) MWCNTs, and (d) GON. Enzyme retained specific activity and kinetics depend on the nanosupport characteristics, both physical and chemical.

maximum rate of reaction), K_m (i.e., Michaelis–Menten constant), and k_{cat} (i.e., enzyme turnover) were calculated using nonlinear regression[36,59] and compared with the kinetic parameters of the free enzyme in solution (Table 1). The V_{max} of SBP physically immobilized onto MWCNTs decreased by 87%, while the V_{max} of the SBP immobilized onto GON decreased by about 98% relative to V_{max} of free enzyme in solution. K_m values of the immobilized SBP also showed an overall decrease however within the same order of magnitude with the K_m values of the free enzyme. The catalytic efficiency (k_{cat}/K_m) of the immobilized enzyme (generally used as a comparator for the rate at which the immobilized enzyme catalytically transforms its substrate)[36,60] was much lower than that of the free SBP and varied both with the nanosupport and immobilization technique being used. For example, the catalytic efficiencies of SBP covalently bound onto SWCNTs, MWCNTs and GON were about 10%, 11%, and 3% of that of the free enzyme in solution. Further, the lowest activity of immobilized SBP was obtained at the flat surface of GON.

The observed changes in the kinetic parameters indicate that the different characteristics of the nanosupports influenced directly the catalytic behavior of the immobilized enzyme. Even though no significant changes in the enzyme active site conformation occurred (i.e., the K_m of the immobilized enzymes were in the same order of magnitude with the ones of the corresponding free enzymes), the multipoint attachment resulted from the enzyme physical binding could explain both the decrease in the rate of reaction and the reduced catalytic efficiency. In particular, the multipoint attachment led to decreased substrate-binding ability for the immobilized enzyme relative to free enzyme in solution.[11,47−49,61]

These results are in agreement with previous reports that showed that enzymes immobilized onto nanosupports with smaller diameters and thus higher radii of curvature (i.e. SWCNTs (0.8−1.2 nm) or MWCNTs (10−20 nm) relative to GON (500−5000 nm)) tend to retain higher levels of activity.[11,62,63] Higher radius of curvature of the nanosupports ensures an increased center-to-center distance between two adjacent immobilized enzymes (Figure 2b), which could potentially reduce the unwanted interactions between neighboring proteins and also reduce their multi-attachment points to the nanosupports. Contrary to that, increased protein−protein interactions caused by a less curved surface could result in a more dramatic activity loss over time and in a harsh environment.[11,12,36,63]

The nanosupport's curvature trend was not confirmed for the enzyme immobilized onto SWCNTs relative to the enzyme immobilized onto MWCNTs; in particular, SBP showed the highest enzyme activity at the MWCNTs interface which has a larger radius of curvature than that of the SWCNTs. The apparent discrepancy in the reported results is due to the bio−nano interface being also influenced by the enzyme structure and its surface energy.[24] Specifically, at the working pH (PBS pH 7), SBP carries a negative charge (pI 3.9).[64] The presence of a larger density of COOH groups onto the MWCNTs surface effectively lowers their pI more so than that of the SWCNTs.[65] Thus, the SWCNTs will carry a weaker negative charge compared to that of the MWCNTs leading to less repulsion of the enzyme at their nanointerface. This effect coupled with the relatively large dimensions of the SBP (6.1 nm × 3.5 nm × 4.0 nm)[66] when compared to the diameter of the SWCNTs (0.8−1.2 nm) could also lead to an increase in protein−protein interactions and thus account for the lower activity and reduced catalytic efficiency as observed at this nanointerface.

Table 1. Soybean Peroxidase (SBP) Michaelis–Menten Kinetics

nanosupport and immobilization method	V_{max} (μM/μg s)	K_m (μM)	k_{cat} (1/s)	k_{cat}/K_m
SWCNTs (physical)	0.005 ± 0.001	3.7 ± 1.0	0.14 ± 0.04	0.04 ± 0.02
SWCNTs (covalent)	0.012 ± 0.003	1.9 ±0.7	0.33 ± 0.12	0.20 ± 0.07
SWCNTs (covalent with PEG)	0.022 ± 0.011	1.9 ± 0.8	0.61 ± 0.43	0.33 ± 0.09
MWCNTs (physical)	0.017 ± 0.007	7.2 ± 2.3	0.47 ± 0.27	0.07 ± 0.02
MWCNTs (covalent)	0.011 ± 0.004	1.6 ± 0.4	0.30 ± 0.16	0.22 ± 0.13
MWCNTs (covalent with PEG)	0.008 ± 0.003	2.9 ± 0.4	0.22 ± 0.12	0.08 ± 0.03
GON (physical)	0.003 ± 0.001	1.4 ± 1.0	0.08 ± 0.04	0.12 ± 0.13
GON (covalent)	0.005 ± 0.001	2.6 ± 0.3	0.14 ± 0.04	0.06 ± 0.01
GON (covalent with PEG)	0.002 ± 0.001	2.8 ± 2.7	0.03 ± 0.04	0.02 ± 0.02
free SBP	0.128 ± 0.042	1.9 ± 0.8	3.53 ± 1.64	2.01 ± 0.63

Specificity of the Bio–Nano-Interface Reaction. To assess whether there is a symbiotic relationship between the immobilized enzyme and nanomaterial characteristics that influence such catalytic behavior at nanointerfaces and whether there is an optimal nanosupport that can be used when aiming to preserve enzyme catalytic behavior, we extended our initial study of the SBP to two additional biocatalysts, namely chloroperoxidase (CPO) and glucose oxidase (GO_X). The additional studies however excluded GON as a nanosupport because of the low activity and increased protein–protein interactions observed when SBP was used as an example.

Our complementary studies confirmed that MWCNTs nanosupports provided once again the optimum nanointerfaces to preserve the additionally selected two-enzyme catalytic behavior and activities. In particular, CPO bound onto MWCNTs retained about 29%, 49%, and 30% specific activities after physical adsorption, covalent binding, and covalent binding through the PEG linker, respectively, when compared to free enzyme in solution (Supporting Information Table S3). These specific activities were ∼27%, 46%, and 27% higher for each respective immobilization method when compared to the specific activity of the enzyme immobilized onto SWCNTs. Further, covalent binding onto MWCNTs seemed to have benefited CPO more than it benefited SBP. This was presumably due to the higher ability of CPO to bind away from its active site when compared to SBP. Specifically, even though both enzymes have similar sizes and molecular weights,[24,25,67] the different mapping of their amino acid sequences as well as their different number of lysine groups (five lysine for CPO and only three for SBP) influenced their different binding ability at nanointerfaces. Furthermore, at the working pH values, i.e., CAB (pH 4.8) for CPO (pI 4.0) and PBS (pH 7) for SBP (pH 3.9), each enzyme is negatively charged, but SBP is more so.[64,68] Lastly, the decrease in activity observed upon utilization of the PEG linker was attributed to the nonspecific interactions of the PEG linker with the active site of both CPO and SBP containing histidine groups. Specifically, studies have shown that histidine group interactions with PEG could potentially lead to substrate inhibition and decreased enzyme activity.[69,70] The greater impact seen for CPO is presumably due to the inherent rigidity of its active site when compared to the more flexible one of SBP.[69,71]

The kinetic behavior of the immobilized CPO (Supporting Information Table S4) was also assessed using varying concentrations of hydrogen peroxide (Figure 4a–c). The V_{max} of CPO covalently immobilized onto MWCNTs was larger than that of the enzyme immobilized through both physical and covalent through the PEG linker techniques. K_m values for the immobilized CPO were on the same order of magnitude as for the free enzyme, indicating that no significant enzyme active site conformational change occurred upon immobilization. Further, k_{cat}/K_m catalytic efficiency of the CPO physically immobilized onto SWCNTs and MWCNTs decreased to about 99% and 78% relative to the catalytic efficiency of the free enzyme.

The more complex and larger GO_X (6.0 nm × 5.2 nm × 7.7 nm)[72] showed however an increase in the retained specific activity upon immobilization using covalent binding, with a further increase upon the utilization of the PEG linker (Supporting Information Table S5). Namely, GO_X bound to MWCNTs physically, covalently, and covalently with the PEG linker resulted in retained specific activities of around 20%, 44%, and 63%, respectively, relative to the activity of the free enzyme in solution. The active site inhibition was less likely to occur in the GO_X trials due to its extended numbers of lysine residues (i.e., 60 lysine groups present on the enzyme structure compared to only five or three for CPO and SBP, respectively)[73] that would thus offer multiple binding sites for the specific covalent immobilization. Further, the benefit of the PEG linker was obvious for this large enzyme, presumably due to the reduced interactions of the GO_X or reduced enzyme–enzyme interactions at the nanosupports.[11,74,75]

The catalytic behavior of the immobilized GO_X (Supporting Information Table S6) was also evaluated using varying concentrations of glucose (Figure 4d–f). Specifically, GO_X bound to MWCNTs physically, covalently, and covalently through a PEG linker yielded V_{max} values of around 0.098, 0.218, and 0.234, respectively. These trends correspond to those resulting from specific retained activity determination. K_m values for GO_X were on the same order of magnitude as for the free enzyme, confirming that there was no significant enzyme active site conformational change upon immobilization.

Optimum Nanosupport for Optimum Catalytic Behavior. Our studies showed that the impact on enzyme binding at nanosupport interfaces is a function of both the enzyme and the nanosupport characteristics. Thus, in order to ensure maximum catalytic efficiency of bio–nano conjugates for selected applications, there is an optimum nanosupport and an optimum immobilization method to be used. For instance, our results have shown that nanosupports of MWCNTs 10–20 nm in diameter functionalized with COOH groups are the most suitable for being used for immobilization of enzymes with a footprint of half of this diameter or as large as the nanosupport itself (Table 2). Further, our results have shown that the catalytic behavior of the enzymes upon immobilization is a function of the overall enzyme isoelectric properties and changes in the surrounding environment. While our studies have used three selected enzymes and three selected nanosupports, they can further be extended to identify the best parameters and thus conditions to be considered for synthetic applications of such biocatalyst-based conjugates.

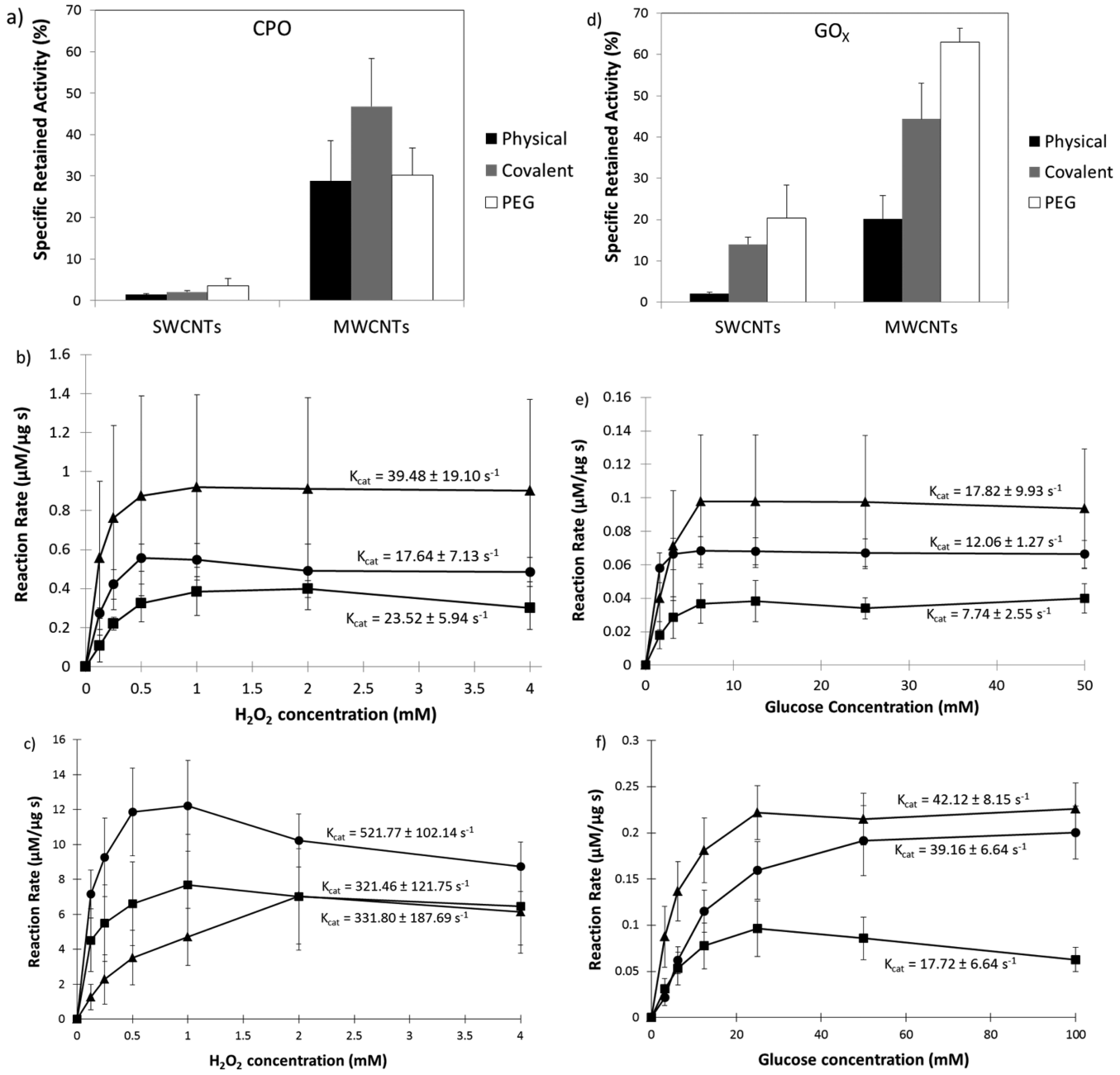

Figure 4. Catalytic behavior of chloroperoxidase (CPO) and glucose oxidase (GO_X) immobilized onto different nanosupports. (a) Specific retained activity comparison of the CPO immobilized onto SWCNTs and MWCNTs via physical adsorption, covalent binding, and covalent binding via PEG linker. Michaelis–Menten kinetics of CPO immobilized using physical adsorption (filled square), covalent binding (filled circle), and covalent binding via PEG linker (filled triangle) onto (b) SWCNTs and (c) MWCNTs. (d) Specific retained activity comparison of GO_X immobilized onto SWCNTs and MWCNTs via physical adsorption, covalent binding, and covalent binding via PEG linker. Michaelis–Menten kinetics data of GO_X immobilized using physical adsorption (filled square), covalent binding (filled circle), and covalent binding via PEG linker (filled triangle) onto (e) SWCNTs and (f) MWCNTs.

Table 2. MWCNT-Based Conjugates as Optimum Nanosupports to Provide High Catalytic Behavior

enzyme (immobilization method)	V_{max} (μM/μg s)	K_m (μM)	k_{cat} (1/s)	k_{cat}/K_m
SBP (covalent)	0.011 ± 0.004	1.6 ± 0.4	0.30 ± 0.16	0.22 ± 0.13
CPO (covalent)	12.42 ± 2.43	120 ± 8	521.77 ± 102.14	4.48 ± 0.86
GO_X (covalent with PEG)	0.234 ± 0.032	2600 ± 700	42.12 ± 8.15	0.018 ± 0.008

For instance, one can envision comparing even lower surface curvatures (i.e., spheres or gold nanorods) in order to understand how nanomaterial characteristics and physico-chemical properties and the interplay at the enzyme–nanosupport interface, as well as the symbiotic reactions that take place at this interface, can be tailored to lead to maximum retained enzyme activity while augmenting recovery of active enzyme–nanomaterial conjugates. Providing user-directed feedback for individual

dx.doi.org/10.1021/am500773g | ACS Appl. Mater. Interfaces 2014, 6, 5393–5403

application, and accounting for biochemical data relaying on the characteristics of both the nanosupport and the biocatalyst being tested, is empirically necessary for enzymes immobilized onto carbon-based nanosupports to reach their full operational potential.

CONCLUSIONS

We showed that controlling the interplay as well as the symbiotic reactions that take place at the enzyme−carbon-based nanointerfaces lead to enzyme-based conjugates with higher catalytic behavior. In particular, we showed that activity of the enzyme−carbon-based conjugates can be tuned by the user by controlling the immobilization conditions, the local curvature of the nanosupport, and its physico-chemical properties. Further, our studies showed that user manipulation of the immobilization conditions as well as careful nanosupport and enzyme selection are required for the optimum catalytic efficiency of these conjugates. The detailed characterization and optimization of the enzyme−nanointerface reactions will potentially result in improved interfacial interactions, stable catalytic behaviors, and thus a greater understanding of the molecular requirements and symbiotic reactions at such interfaces for integrated technological applications of bio−nano conjugates in pharmacological industry, biosensors, biofuel cells and bioactive coatings formation.

ASSOCIATED CONTENT

Supporting Information

In-depth characterization of the carbon-based nanomaterials used in this study. Briefly, Figure S1 contains the SEM images of these carbon-based nanomaterials, while Table S1 contains the nanomaterial dispersity analysis. Tables S2−S6 contain information on the loading, activity data, and Michaelis−Menten kinetics for each individual enzyme−nanosupport configuration. This material is available free of charge via the Internet at http://pubs.acs.org.

AUTHOR INFORMATION

Corresponding Author

*Mailing address: Department of Chemical Engineering, West Virginia University, Benjamin M. Statler College of Engineering and Mineral Resources, P.O. Box 6102, Morgantown, WV 26506, United States. E-mail: cerasela-zoica.dinu@mail.wvu.edu. Tel.: 1 304 293 9338. Fax: 1 304 293 4139.

Notes

The authors declare no competing financial interest.

ACKNOWLEDGMENTS

This work was supported by the National Science Foundation (NSF-CBET: 1033266). The authors acknowledge NanoSAFE and WVU Chemical Engineering for the shared facilities. The authors thank undergraduate Andrew Maloney for his involvement in the initial stage of the project.

REFERENCES

(1) Mateo, C.; Palomo, J. M.; Fernandez-Lorente, G.; Guisan, J. M.; Fernandez-Lafuente, R. Improvement of Enzyme Activity, Stability and Selectivity via Immobilization Techniques. *Enzyme. Microb. Tech.* **2007**, *40*, 1451−1463.

(2) Rodrigues, R. C.; Ortiz, C.; Berenguer-Murcia, A.; Torres, R.; Fernandez-Lafuente, R. Modifying Enzyme Activity and Selectivity by Immobilization. *Chem. Soc. Rev.* **2013**, *42*, 6290−6307.

(3) Wang, X. Q.; Wang, Q. H.; Liu, Y. Y.; Ma, H. Z. On-Site Production of Crude Glucoamylase for Kitchen Waste Hydrolysis. *Waste Manage. Res.* **2010**, *28*, 539−544.

(4) Mao, X.; Buchanan, I. D.; Stanley, S. J. Development of an Integrated Enzymatic Treatment System for Phenolic Waste Streams. *Environ. Technol.* **2006**, *27*, 1401−1410.

(5) Zaks, A. Industrial Biocatalysis. *Curr. Opin. Chem. Biol.* **2001**, *5*, 130−136.

(6) Verma, M. L.; Barrow, C. J.; Puri, M. Nanobiotechnology as a Novel Paradigm for Enzyme Immobilisation and Stabilisation with Potential Applications in Biodiesel Production. *Appl. Microbiol. Biot.* **2013**, *97*, 23−39.

(7) Wandrey, C.; Liese, A.; Kihumbu, D. Industrial Biocatalysis: Past, Present, and Future. *Org. Process. Res. Dev.* **2000**, *4*, 286−290.

(8) Yang, M. L.; Wang, J.; Li, H. Q.; Zheng, J. G.; Wu, N. Q. N. A Lactate Electrochemical Biosensor with a Titanate Nanotube as Direct Electron Transfer Promoter. *Nanotechnology* **2008**, *19*, 1−6.

(9) Cui, Y. L.; Zhang, B.; Liu, B. Q.; Chen, H. F.; Chen, G. N.; Tang, D. P. Sensitive Detection of Hydrogen Peroxide in Foodstuff Using an Organic-Inorganic Hybrid Multilayer-Functionalized Graphene Biosensing Platform. *Microchim. Acta* **2011**, *174*, 137−144.

(10) Kumar, S.; Jana, A. K.; Dhamija, I.; Maiti, M. Chitosan-Assisted Immobilization of Serratiopeptidase on Magnetic Nanoparticles, Characterization and Its Target Delivery. *J. Drug. Target.* **2014**, *22*, 123−137.

(11) Dinu, C. Z.; Zhu, G.; Bale, S. S.; Anand, G.; Reeder, P. J.; Sanford, K.; Whited, G.; Kane, R. S.; Dordick, J. S. Enzyme-Based Nanoscale Composites for Use as Active Decontamination Surfaces. *Adv. Funct. Mater.* **2010**, *20*, 392−398.

(12) Grover, N.; Borkar, I. V.; Dinu, C. Z.; Kane, R. S.; Dordick, J. S. Laccase- and Chloroperoxidase-Nanotube Paint Composites with Bactericidal and Sporicidal Activity. *Enzyme Microb. Tech.* **2012**, *50*, 271−279.

(13) Besteman, K.; Lee, J. O.; Wiertz, F. G. M.; Heering, H. A.; Dekker, C. Enzyme-Coated Carbon Nanotubes as Single-Molecule Biosensors. *Nano Lett.* **2003**, *3*, 727−730.

(14) Luckarift, H. R.; Spain, J. C.; Naik, R. R.; Stone, M. O. Enzyme Immobilization in a Biomimetic Silica Support. *Nat. Biotechnol.* **2004**, *22*, 211−213.

(15) Hernandez, K.; Fernandez-Lafuente, R. Control of protein immobilization: Coupling Immobilization and Site-Directed Mutagenesis to Improve Biocatalyst or Biosensor Performance. *Enzyme Microb. Tech.* **2011**, *48*, 107−122.

(16) Garcia-Galan, C.; Berenguer-Murcia, A.; Fernandez-Lafuente, R.; Rodrigues, R. C. Potential of Different Enzyme Immobilization Strategies to Improve Enzyme Performance. *Adv. Synth. Catal.* **2011**, *353*, 2885−2904.

(17) Dinu, C. Z.; Borkar, I. V.; Bale, S. S.; Campbell, A. S.; Kane, R. S.; Dordick, J. S. Perhydrolase-Nanotube-Paint Sporicidal Composites Stabilized by Intramolecular Crosslinking. *J. Mol. Catal. B−Enzym.* **2012**, *75*, 20−26.

(18) Wu, J. C.; Lee, S. S.; Mahmood, M. M. B.; Chow, Y.; Talukder, M. M. R.; Choi, W. J. Enhanced Activity and Stability of Immobilized Lipases by Treatment with Polar Solvents Prior to Lyophilization. *J. Mol. Catal. B−Enzym.* **2007**, *45*, 108−112.

(19) Asuri, P.; Bale, S. S.; Pangule, R. C.; Shah, D. A.; Kane, R. S.; Dordick, J. S. Structure, Function, and Stability of Enzymes Covalently Attached to Single-Walled Carbon Nanotubes. *Langmuir* **2007**, *23*, 12318−12321.

(20) Aburto, J.; Ayala, M.; Bustos-Jaimes, I.; Montiel, C.; Terres, E.; Dominguez, J. M.; Torres, E. Stability and Catalytic Properties of Chloroperoxidase Immobilized on SBA-16 Mesoporous Materials. *Micropor. Mesopor. Mater.* **2005**, *83*, 193−200.

(21) Ivanova, E. P.; Wright, J. P.; Pham, D. K.; Brack, N.; Pigram, P.; Alekseeva, Y. V.; Demyashev, G. M.; Nicolau, D. V. A Comparative Study Between the Adsorption and Covalent Binding of Human Immunoglobulin and Lysozyme on Surface-Modified Poly(tert-butyl methacrylate). *Biomed. Mater.* **2006**, *1*, 24−32.

(22) Bayramoglu, G.; Kiralp, S.; Yilmaz, M.; Toppare, L.; Arica, M. Y. Covalent Immobilization of Chloroperoxidase onto Magnetic Beads: Catalytic Properties and Stability. *Biochem. Eng. J.* **2008**, *38*, 180−188.
(23) Gray, J. S. S.; Montgomery, R. The N-Glycosylation Sites of Soybean Seed Coat Peroxidase. *Glycobiology* **1997**, *7*, 679−685.
(24) Henriksen, A.; Mirza, O.; Indiani, C.; Teilum, K.; Smulevich, G.; Welinder, K. G.; Gajhede, M. Structure of Soybean Seed Coat Peroxidase: A Plant Peroxidase with Unusual Stability and Haem-Apoprotein Interactions. *Protein Sci.* **2001**, *10*, 108−115.
(25) Sundaramoorthy, M.; Terner, J.; Poulos, T. L. The Crystal Structure of Chloroperoxidase: A Heme Peroxidase-Cytochrome P450 Functional Hybrid. *Structure* **1995**, *3*, 1367−1377.
(26) Wilson, R.; Turner, A. P. F. Glucose-Oxidase - an Ideal Enzyme. *Biosens. Bioelectron.* **1992**, *7*, 165−185.
(27) Galende, P. P.; Munoz, T. M.; Roig, M. G.; de Maria, C. G. Use of Crude Extract of Lentil Plant (Lens culinaris Medikus) in Peroxidase-Based Analyses: Fast Kinetic Determination of Hydrogen Peroxide and Sarcosine in Urine. *Anal. Bioanal. Chem.* **2012**, *404*, 2377−2385.
(28) Bassi, A. S.; McGrath, C. Carbon Paste Biosensor Based on Crude Soybean Seed Hull Extracts for Phenol Detection. *J. Agr. Food Chem.* **1999**, *47*, 322−326.
(29) Wang, B. Q.; Li, B.; Cheng, G. J.; Dong, S. J. Acid-Stable Amperometric Soybean Peroxidase Biosensor Based on a Self-Gelatinizable Grafting Copolymer of Polyvinyl Alcohol and 4-Vinylpyridine. *Electroanal.* **2001**, *13*, 555−558.
(30) Wilberg, K.; Assenhaimer, C.; Rubio, J. Removal of Aqueous Phenol Catalysed by a Low Purity Soybean Peroxidase. *J. Chem. Technol. Biot.* **2002**, *77*, 851−857.
(31) Bodalo, A.; Gomez, J. L.; Gomez, E.; Hidalgo, A. M.; Gomez, M.; Yelo, A. M. Removal of 4-Chlorophenol by Soybean Peroxidase and Hydrogen Peroxide in a Discontinuous Tank Reactor. *Desalination* **2006**, *195*, 51−59.
(32) Patapas, J.; Al-Ansari, M. M.; Taylor, K. E.; Bewtra, J. K.; Biswas, N. Removal of Dinitrotoluenes from Water via Reduction with Iron and Peroxidase-Catalyzed Oxidative Polymerization: A Comparison Between Arthromyces ramosus Peroxidase and Soybean Peroxidase. *Chemosphere* **2007**, *67*, 1485−1491.
(33) Wang, L. M.; Wu, J. Y.; Jiang, Y. C.; Hu, M. C.; Li, S. N.; Zhai, Q. G. Asymmetry Synthesis of Chiral Sulfoxide Catalyzed by Chloroperoxidase. *Acta Chim. Sinica* **2012**, *70*, 465−470.
(34) Wu, J. Y.; Liu, C.; Jiang, Y. C.; Hu, M. C.; Li, S. N.; Zhai, Q. G. Synthesis of Chiral Epichlorohydrin by Chloroperoxidase-Catalyzed Epoxidation of 3-Chloropropene in the Presence of an Ionic Liquid as Co-Solvent. *Catal. Commun.* **2010**, *11*, 727−731.
(35) Zhi, L. F.; Jiang, Y. C.; Hu, M. C.; Li, S. N. Applications of Chloroperoxidase in Chiral Organic Synthesis. *Prog. Chem.* **2006**, *18*, 1150−1156.
(36) Campbell, A. S.; Dong, C. B.; Dordick, J. S.; Dinu, C. Z. BioNano Engineered Hybrids for Hypochlorous Acid Generation. *Process Biochem.* **2013**, *48*, 1355−1360.
(37) Terres, E.; Montiel, M.; Le Borgne, S.; Torres, E. Immobilization of Chloroperoxidase on Mesoporous Materials for the Oxidation of 4,6-Dimethyldibenzothiophene, a Recalcitrant Organic Sulfur Compound Present in Petroleum Fractions. *Biotechnol. Lett.* **2008**, *30*, 173−179.
(38) Ayala, M.; Verdin, J.; Vazquez-Duhalt, R. The Prospects for Peroxidase-Based Biorefining of Petroleum Fuels. *Biocatal. Biotransfor.* **2007**, *25*, 114−129.
(39) Tsai, T. W.; Heckert, G.; Neves, L. F.; Tan, Y. Q.; Kao, D. Y.; Harrison, R. G.; Resasco, D. E.; Schmidtke, D. W. Adsorption of Glucose Oxidase onto Single-Walled Carbon Nanotubes and Its Application in Layer-By-Layer Biosensors. *Anal. Chem.* **2009**, *81*, 7917−7925.
(40) Singh, K.; Singh, B. P.; Chauhan, R.; Basu, T. Fabrication of Amperometric Bienzymatic Glucose Biosensor Based on MWCNT Tube and Polypyrrole Multilayered Nanocomposite. *J. Appl. Polym. Sci.* **2012**, *125*, E235−E246.
(41) Min, K.; Ryu, J. H.; Yoo, Y. J. Mediator-free Glucose/O-2 Biofuel Cell Based on a 3-Dimensional Glucose Oxidase/SWNT/Polypyrrole Composite Electrode. *Biotechnol. Bioproc. E* **2010**, *15*, 371−375.
(42) Wong, C. M.; Wong, K. H.; Chen, X. D. Glucose Oxidase: Natural Occurrence, Function, Properties and Industrial Applications. *Appl. Microbiol. Biot.* **2008**, *78*, 927−938.
(43) Zargoosh, K.; Chaichi, M. J.; Shamsipur, M.; Hossienkhani, S.; Asghari, S.; Qandalee, M. Highly Sensitive Glucose Biosensor Based on the Effective Immobilization of Glucose Oxidase/Carbon-Nanotube and Gold Nanoparticle in Nafion Film and Peroxyoxalate Chemiluminescence Reaction of a New Fluorophore. *Talanta* **2012**, *93*, 37−43.
(44) Pavlidis, I. V.; Vorhaben, T.; Tsoufis, T.; Rudolf, P.; Bornscheuer, U. T.; Gournis, D.; Stamatis, H. Development of Effective Nanobiocatalytic Systems through the Immobilization of Hydrolases on Functionalized Carbon-Based Nanomaterials. *Bioresource Technol.* **2012**, *115*, 164−171.
(45) Shan, G. B.; Surampalli, R. Y.; Tyagi, R. D.; Zhang, T. C. Nanomaterials for Environmental Burden Reduction, Waste Treatment, and Nonpoint Source Pollution Control: a Review. *Front. Environ. Sci. En.* **2009**, *3*, 249−264.
(46) Demarche, P.; Junghanns, C.; Nair, R. R.; Agathos, S. N. Harnessing the Power of Enzymes for Environmental Stewardship. *Biotechnol. Adv.* **2012**, *30*, 933−953.
(47) Rodrigues, R. C.; Bolivar, J. M.; Palau-Ors, A.; Volpato, G.; Ayub, M. A. Z.; Fernandez-Lafuente, R.; Guisan, J. M. Positive Effects of the Multipoint Covalent Immobilization in the Reactivation of Partially Inactivated Derivatives of Lipase from Thermomyces lanuginosus. *Enzyme Microb. Tech.* **2009**, *44*, 386−393.
(48) Nakamoto, M.; Hoshino, Y.; Miura, Y. Effect of Physical Properties of Nanogel Particles on the Kinetic Constants of Multipoint Protein Recognition Process. *Biomacromolecules* **2014**, *15*, 541−547.
(49) Bolivar, J. M.; Rocha-Martin, J.; Mateo, C.; Cava, F.; Berenguer, J.; Vega, D.; Fernandez-Lafuente, R.; Guisan, J. M. Purification and Stabilization of a Glutamate Dehydrogenase from Thermus thermophilus via Oriented Multisubunit Plus Multipoint Covalent Immobilization. *J. Mol. Catal. B−Enzym.* **2009**, *58*, 158−163.
(50) Dong, C. B.; Campell, A. S.; Eldawud, R.; Perhinschi, G.; Rojanasakul, Y.; Dinu, C. Z. Effects of Acid Treatment on Structure, Properties and Biocompatibility of Carbon Nanotubes. *Appl. Surf. Sci.* **2013**, *264*, 261−268.
(51) Stobinski, L.; Lesiak, B.; Kover, L.; Toth, J.; Biniak, S.; Trykowski, G.; Judek, J. Multiwall Carbon Nanotubes Purification and Oxidation by Nitric Acid Studied by the FTIR and Electron Spectroscopy Methods. *J. Alloy Compd.* **2010**, *501*, 77−84.
(52) Guo, H. L.; Wang, X. F.; Qian, Q. Y.; Wang, F. B.; Xia, X. H. A Green Approach to the Synthesis of Graphene Nanosheets. *Acs Nano* **2009**, *3*, 2653−2659.
(53) Wepasnick, K. A.; Smith, B. A.; Schrote, K. E.; Wilson, H. K.; Diegelmann, S. R.; Fairbrother, D. H. Surface and Structural Characterization of Multi-Walled Carbon Nanotubes Following Different Oxidative Treatments. *Carbon* **2011**, *49*, 24−36.
(54) Shieh, Y. T.; Liu, G. L.; Wu, H. H.; Lee, C. C. Effects of Polarity and pH on the Solubility of Acid-Treated Carbon Nanotubes in Different Media. *Carbon* **2007**, *45*, 1880−1890.
(55) Shieh, Y. T.; Chen, J. Y.; Twu, Y. K.; Chen, W. J. The Effect of pH and Ionic Strength on the Dispersion of Carbon Nanotubes in Poly(acrylic acid) Solutions. *Polym. Int.* **2012**, *61*, 554−559.
(56) Brady, D.; Jordaan, J. Advances in Enzyme Immobilisation. *Biotechnol. Lett.* **2009**, *31*, 1639−1650.
(57) Rodrigues, R. C.; Godoy, C. A.; Filice, M.; Bolivar, J. M.; Palau-Ors, A.; Garcia-Vargas, J. M.; Romero, O.; Wilson, L.; Ayub, M. A. Z.; Fernandez-Lafuente, R.; Guisan, J. M. Reactivation of Covalently Immobilized Lipase from Thermomyces lanuginosus. *Process Biochem.* **2009**, *44*, 641−646.
(58) Mateo, C.; Palomo, J. M.; Fuentes, M.; Betancor, L.; Grazu, V.; Lopez-Gallego, F.; Pessela, B. C. C.; Hidalgo, A.; Fernandez-Lorente, G.; Fernandez-Lafuente, R.; Guisan, J. M. Glyoxyl Agarose: A Fully Inert and Hydrophilic Support for Immobilization and High Stabilization of Proteins. *Enzyme Microb. Tech.* **2006**, *39*, 274−280.
(59) Al-Haque, N.; Santacoloma, P. A.; Neto, W.; Tufvesson, P.; Gani, R.; Woodley, J. M. A Robust Methodology for Kinetic Model Parameter

Estimation for Biocatalytic Reactions. *Biotechnol. Progr.* **2012**, *28*, 1186−1196.
(60) Eisenthal, R.; Danson, M. J.; Hough, D. W. Catalytic Efficiency and K(cat) /K-M: A Useful Comparator? *Trends Biotechnol.* **2007**, *25*, 247−249.
(61) Arabaci, G.; Usluoglu, A. Catalytic Properties and Immobilization Studies of Catalase from Malva sylvestris L. *J. Chem.−Ny* **2013**, *2013*, 1−6.
(62) Asuri, P.; Bale, S. S.; Karajanagi, S. S.; Kane, R. S. The Protein-Nanomaterial Interface. *Curr. Opin. Biotech.* **2006**, *17*, 562−568.
(63) Asuri, P.; Karajanagi, S. S.; Yang, H. C.; Yim, T. J.; Kane, R. S.; Dordick, J. S. Increasing Protein Stability through Control of the Nanoscale Environment. *Langmuir* **2006**, *22*, 5833−5836.
(64) Zhang, W. C.; Dai, X. H.; Zhao, Y.; Lu, X. M.; Gao, P. J. Comparison of the Different Types of Surfactants for the Effect on Activity and Structure of Soybean Peroxidase. *Langmuir* **2009**, *25*, 2363−2368.
(65) McPhail, M. R.; Sells, J. A.; He, Z.; Chusuei, C. C. Charging Nanowalls: Adjusting the Carbon Nanotube Isoelectric Point via Surface Functionalization. *J Phys. Chem. C* **2009**, *113*, 14102−14109.
(66) Van Gough, D.; Wolosiuk, A.; Braun, P. V. Mesoporous ZnS Nanorattles: Programmed Size Selected Access to Encapsulated Enzymes. *Nano Lett.* **2009**, *9*, 1994−1998.
(67) Bantleon, R.; Altenbuchner, J.; Vanpee, K. H. Chloroperoxidase from Streptomyces-Lividans - Isolation and Characterization of the Enzyme and the Corresponding Gene. *J. Bacteriol.* **1994**, *176*, 2339−2347.
(68) Han, Y. J.; Watson, J. T.; Stucky, G. D.; Butler, A. Catalytic Activity of Mesoporous Silicate-Immobilized Chloroperoxidase. *J. Mol. Catal. B−Enzym.* **2002**, *17*, 1−8.
(69) Kamal, J. K. A.; Behere, D. V. Activity, Stability and Conformational Flexibility of Seed Coat Soybean Peroxidase. *J. Inorg. Biochem.* **2003**, *94*, 236−242.
(70) Zobnina, V. G.; Kosevich, M. V.; Chagovets, V. V.; Boryak, O. A.; Vekey, K.; Gomory, A.; Kulyk, A. N. Interactions of Oligomers of Organic Polyethers with Histidine Amino Acid. *Rapid Commun. Mass Sp.* **2012**, *26*, 532−540.
(71) Sundaramoorthy, M.; Terner, J.; Poulos, T. L. Stereochemistry of the Chloroperoxidase Active Site: Crystallographic and Molecular-Modeling Studies. *Chem. Biol.* **1998**, *5*, 461−473.
(72) Libertino, S.; Aiello, V.; Scandurra, A.; Renis, M.; Sinatra, F. Immobilization of the Enzyme Glucose Oxidase on Both Bulk and Porous SiO2 Surfaces. *Sensors−Basel.* **2008**, *8*, 5637−5648.
(73) Mossavarali, S.; Hosseinkhani, S.; Ranjbar, B.; Mirohaei, M. Stepwise Modification of Lysine Residues of Glucose Oxidase with Citraconic Anhydride. *Int. J. Biol. Macromol.* **2006**, *39*, 192−196.
(74) Manta, C.; Ferraz, N.; Betancor, L.; Antunes, G.; Batista-Viera, F.; Carlsson, J.; Caldwell, K. Polyethylene Glycol as a Spacer for Solid-Phase Enzyme Immobilization. *Enzyme Microb. Tech.* **2003**, *33*, 890−898.
(75) Sung, W. J.; Bae, Y. H. A Glucose Oxidase Electrode Based on Polypyrrole with Polyanion/PEG/Enzyme Conjugate Dopant. *Biosens. Bioelectron.* **2003**, *18*, 1231−1239.